SYSTEMS BIOLOGY

Systematic inference identifies a major source of heterogeneity in cell signaling dynamics: The rate-limiting step number

Dae Wook Kim[1,2]†‡, Hyukpyo Hong[1,2]†, Jae Kyoung Kim[1,2]*

Identifying the sources of cell-to-cell variability in signaling dynamics is essential to understand drug response variability and develop effective therapeutics. However, it is challenging because not all signaling intermediate reactions can be experimentally measured simultaneously. This can be overcome by replacing them with a single random time delay, but the resulting process is non-Markovian, making it difficult to infer cell-to-cell heterogeneity in reaction rates and time delays. To address this, we developed an efficient and scalable moment-based Bayesian inference method (MBI) with a user-friendly computational package that infers cell-to-cell heterogeneity in the non-Markovian signaling process. We applied MBI to single-cell expression profiles from promoters responding to antibiotics and discovered a major source of cell-to-cell variability in antibiotic stress response: the number of rate-limiting steps in signaling cascades. This knowledge can help identify effective therapies that destroy all pathogenic or cancer cells, and the approach can be applied to precision medicine.

INTRODUCTION

The response of genetically identical cells to the same extracellular signal is largely heterogeneous in both response time and strength, even in a homogeneous environment (*1*–*4*). This cell signaling heterogeneity ultimately leads to diverse, often unpredictable clinical complications, such as drug response variability (*5*), emergence of persister cells (*6*), incomplete penetrance (*7*), and phenotypic plasticity (Fig. 1A) (*8*). One of the major sources of this cell signaling heterogeneity is a difference in cellular phenotypes, such as cell cycle phase (*9*), cell growth rate (*10*), or asymmetric cell division (*11*). Another major source is heterogeneity in the signal cascades, such as the number of signaling receptors (*12*) and the kinetics of numerous intermediate signaling reactions (*1*, *13*). However, while cellular phenotypes can be tracked with flow cytometry, microfluidics, and time-lapse microscopy (*11*, *14*), only a few steps of signaling cascades can usually be tracked in a single cell, for example, with multicolor luciferase reporter assays (*15*–*17*).

Because of this limit of the data, intermediate signaling kinetics are unidentifiable (Fig. 1B, i). One promising way to circumvent this is to replace a chain of hidden intermediate steps with a single random time delay (Fig. 1B, ii) (*18*–*22*). This allows one to describe signaling cascades with a chain of hidden steps by using a simple delayed birth-death process having only one variable that is observable experimentally: birth (i.e., signal activation), delay (i.e., signal transduction), and death (i.e., decay of observable signaling molecule) (Fig. 2A) (*23*). However, because this model is non-Markovian (i.e., the formation of the response molecule depends on past signal activation events due to a time delay as well as the current status of a system), well-established inference machinery based on the Markov property (i.e., memoryless; the formation of the response molecule depends only on the current state not on the past) cannot be directly applied (*24*). Recently, meaningful progress has been made: A Bayesian inference method based on non-Markovian delay chemical master equations (CMEs) describing the time evolution of stochastic systems with delay has been developed (Box 1) (*20*). However, this framework rests on the assumption that all time trace measurements are obtained from identical cells with the same biochemical parameters, and thus it cannot be used to quantify the heterogeneity in signaling parameters (e.g., signal transduction delay) across cells. This challenge can be overcome with a mixed-effects modeling approach that offers a framework to analyze cell population–level data and accounts for cell-to-cell heterogeneity in the population (*25*, *26*). However, its potential in non-Markovian delayed systems has yet to be realized.

The other limitation of the previous methods based on CMEs is computational intractability. Because they track whole probabilities over the integer-valued state space of molecule counts, inference using them is substantially slowed when the amount of provided data increases (*20*, *27*). One possible remedy for this might be to use low-order moments of data (e.g., mean) instead of all the individual data points (Fig. 1B, iii) (*28*). Specifically, tracking the mean number of molecules, which includes the essential information for determining the model parameters, does not increase the amount of the data used for parameter estimation and thus computational cost, although the number of measurements (i.e., total data points) increases. However, derivation of exact moments is challenging in non-Markovian delayed models as the conditional probabilities, describing the effect of the models' history (i.e., past model dynamics) on the present model dynamics, need to be handled (*29*). Thus, the approximate moments have been used under the assumption that the number of molecules is large (*30*).

Here, we developed an exact moment-based Bayesian inference method (MBI) for signaling processes of a heterogeneous cell population by using a mixed-effects modeling approach (*25*) and deriving exact moments of the process. It can accurately capture the cell-to-cell heterogeneous birth and death rates and delays for both signal transduction and feedback. Furthermore, MBI can be applied

[1]Department of Mathematical Sciences, Korea Advanced Institute of Science and Technology, Daejeon 34141, Republic of Korea. [2]Biomedical Mathematics Group, Institute for Basic Science, Daejeon 34126, Republic of Korea.
*Corresponding author. Email: jaekkim@kaist.ac.kr
†These authors contributed equally to this work.
‡Present address: Department of Mathematics, University of Michigan, Ann Arbor, MI 48109, USA.

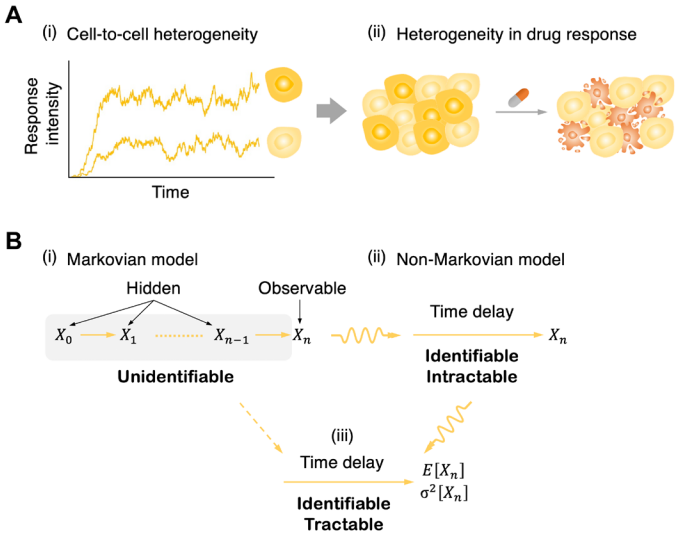

Fig. 1. A framework for inference of cell signaling cascades with a chain of hidden reaction steps. (**A**) Given extracellular signals, genetically identical cells respond differently even in a homogeneous environment (i). This cell-to-cell heterogeneity yields heterogeneous therapeutic response (ii). (**B**) In cell signaling cascades, intermediates (X_0~X_{n-1}) are experimentally unobservable (i.e., hidden), and only the final output, X_n, is observable (i). Because the intermediate kinetics are unidentifiable, a chain of intermediate reaction steps needs to be simplified with a single random time delay (ii). However, the simplified system becomes non-Markovian, and thus the inference of its dynamics is mathematically and computationally intractable. This can be circumvented by exploiting low-order moments (i.e., mean and variance) including key information of the dynamics (iii).

to large data as it uses only the first moments of large data rather than all individual data points. We used MBI to analyze previously published single-cell profiles of time-lapse fluorescent protein expression from various promoters in response to four antibiotic stresses: tetracycline (TET), trimethoprim (TMP), nitrofurantoin (NIT), and chloramphenicol (CHL) in an *Escherichia coli* (*E. coli*) population (*2*, *3*). This revealed large cell-to-cell variability in stress signal activation rate and transduction delay. Importantly, our systematic inference results identified a previously unrecognized parameter that causes cell-to-cell variability in response to antibiotic stress signals: the number of rate-limiting steps in the signal transduction cascade. This was unexpected because a large number of rate-limiting steps have been known to reduce the intracellular variability in transduction delay (*3*, *31*). Our finding of the major source of cell-to-cell variability in signaling dynamics is critical for developing more potent drugs that kill all target cells, which is important for curing cancer and many infectious diseases (*4*, *32*). Our approach provides an important step toward elucidating cell-to-cell variability in signal dynamics, such as in response to cytotoxic drugs.

RESULTS

Cellular processes with hidden reactions can be described with a gamma-distributed delayed model

After plasma membrane receptors are activated by an extracellular signal (Fig. 2A, i, red arrow), the signal is transduced through a chain of many intermediate reaction steps (Fig. 2A, i, yellow and gray arrows) and triggers a response whose intensity decays (Fig. 2A, i, blue arrow) (*33*). Among all the intermediate reaction steps, the slowest steps that determine the overall speed of signaling, called rate-limiting steps (Fig. 2A, i, yellow arrows), mainly control the signaling dynamics (*34*). The rate-limiting steps have been widely described as a chain of reversible activation and deactivation of signaling molecules (Fig. 2A, ii; see Supplementary Text A) (*19*, *35*). Specifically, upon initial signal activation with a rate of λ_a, the first inactive intermediate is activated and transformed into its active form, X_0, and then it activates the next inactive intermediate. Throughout such sequential activation of intermediates with a rate of a_i, the initial signal is amplified and, finally, triggers the activation of the last response molecule, X_n. Each active intermediate is deactivated with a rate of r and the last response molecule decays with a rate of λ_d. Note that the time for each reaction step is assumed to be the same as $t_r = r^{-1}$, because all the steps are rate-limiting ones whose time scale is similarly slow [see (*35*) for details].

In this system, typically, only the final output, X_n, can be measured (*16*, *17*). Thus, to handle the limited experimental data, the model with the hidden intermediates (X_0~X_{n-1}) (Fig. 2A, ii) has been simplified to a compact coarse-grained model with the only observable X_n (Fig. 2A, iii; see Supplementary Text A) (*19*, *35*). In the model, the activation of X_n with the signal amplified throughout the intermediate steps is simply described with a rate of $\lambda_b = \lambda_a \prod_{i=1}^{n} \left(\frac{a_i}{r}\right)$. This activation is not immediate but delayed due to the intermediate rate-limiting steps. The time delay (i.e., the time of the signal transduction between signal activation and response), τ, can be shown to follow a gamma distribution, $\Gamma(n, t_r)$, where n and t_r are the number of intermediate rate-limiting steps and the time for each step, respectively (see Supplementary Text A). Similarly, various systems with hidden intermediates such as the protein maturation process (Fig. 2B, i) (*36*) can also be described with a gamma-distributed delayed one-variable model (Fig. 2B, ii and iii; see Supplementary Text A).

Derivation of exact moments of a stochastic delayed birth-death process

While the delayed one-variable model (Fig. 2A, iii and B, iii) is apparently simple, the model is non-Markovian. Thus, its underlying kinetics cannot be inferred with well-established inference machinery based on the Markov property (*37*). Because of this limitation, the time delay has been widely estimated using time points when response time traces first reach a certain threshold level (i.e., first passage time) after signal activation (*2*, *3*, *38*). However, as the first passage time distribution strongly depends on the choice of the threshold (Fig. 2C, top), the mean time delay, μ_τ, estimated using the first passage time so does (Fig. 2C, bottom). Moreover, the standard deviation of time delay, σ_τ, is seriously underestimated. This highlights the need of a systematic inference method for the non-Markovian model with the time delay.

To develop a systematic inference method for the non-Markovian model, we first applied the Transient Little's Law (*39*) and the Chemical Fluctuation Theorem (*21*) to the equivalent queuing process, namely, a delayed birth-death process (Fig. 2D) (*20*, *40*). In the process, birth events are initiated, which follow a Poisson arrival process with the mean birth rate, λ_b (Fig. 2D, red arrows), and they are completed independently after gamma-distributed delay, τ~$\Gamma(n, t_r)$ (Fig. 2D, yellow arrows). Then, death events occur independently, which follow a Poisson arrival process with the mean death rate, λ_d (Fig. 2D, blue arrows). This allowed us to derive the time-varying exact low-order moments, mean, $\mu(t)$, and variance, $\sigma^2(t)$, of X_n

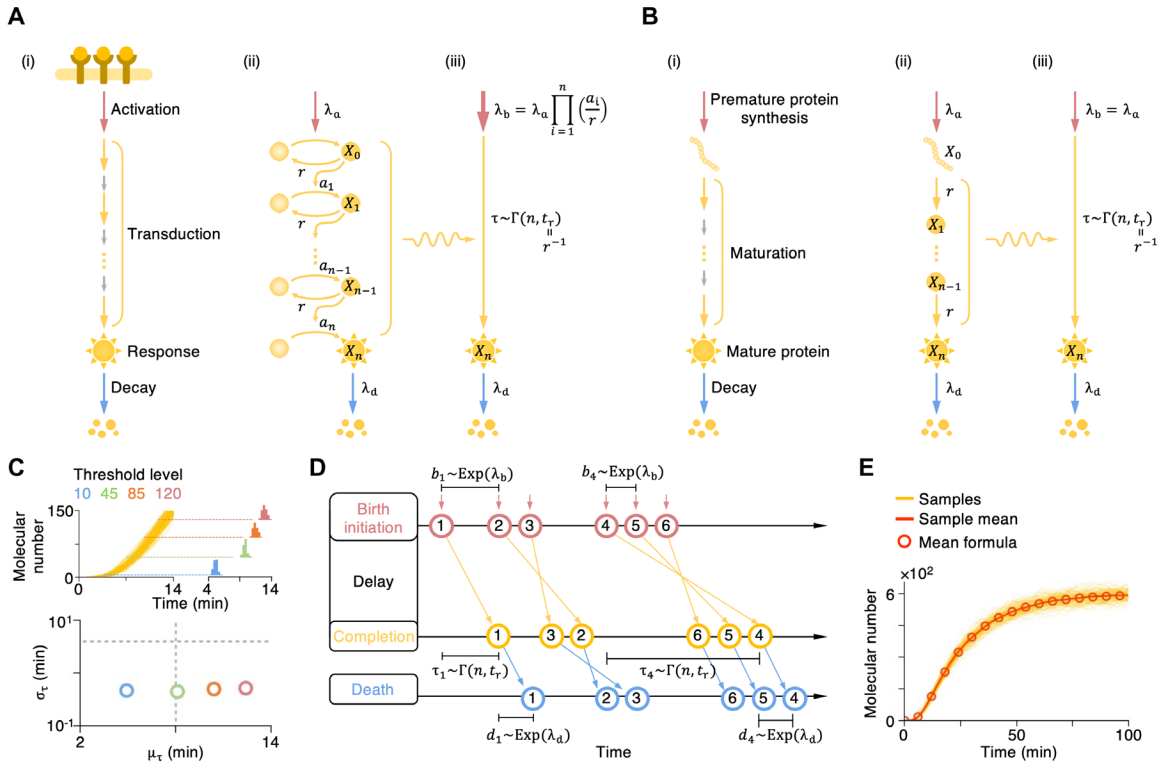

Fig. 2. Sequential biological processes can be described with a delayed birth-death process. (**A**) The activated signal (red arrow, i) is transduced via a chain of intermediate steps (yellow and gray arrows, i) and then triggers a response whose intensity decays (blue arrow, i). This process is mainly regulated by the slowest intermediate steps determining the overall signaling speed (i.e., rate-limiting steps; yellow arrows, i). The dynamics with the rate-limiting steps can be described with a chain of reversible activation and deactivation of signaling molecules (ii). The time to pass through the rate-limiting steps can be simply described with a gamma-distributed delay (iii) (see Supplementary Text A for details). The signal amplification throughout the steps can also be described with the modified signal activation rate, λ_b (iii). (**B**) Protein maturation process with rate-limiting steps (i and ii) can be described with a gamma-distributed delayed one-variable model (iii) (see Supplementary Text A for details). (**C**) The simulated 10^2 sample time traces of the simplified model with delay [A (iii) and B (iii)]. Depending on the subjective choice of a threshold level, the first passage times across the threshold largely change. Vertical and horizontal gray dotted lines represent the true mean and standard deviation of time delay, respectively. (**D**) The dynamics of the simplified model [A (iii) and B (iii)] can be described with a queuing process, namely a delayed birth-death process (*20*, *40*). (**E**) The mean molecular number of the delayed birth-death process calculated by the formula (Eq. 1) (red circle) is the same as that of simulated 10^2 sample time traces (red line). In (C) and (E), $\lambda_b = 30\ \text{min}^{-1}$, $\lambda_d = 0.05\ \text{min}^{-1}$, $n = 4$, and $t_r = 2$ min.

$$\mu(t) = \sigma^2(t) = \frac{\lambda_b}{\lambda_d}\left(\int_0^t g(\tau)\,d\tau - \exp(-\lambda_d t)\int_0^t g(\tau)\exp(\lambda_d \tau)\,d\tau\right) \quad (1)$$

where $g(\tau)$ is the probability density function of $\tau \sim \Gamma(n, t_r)$ (see Supplementary Texts A and B). Note that the mean and variance are the same (i.e., Poissonian). Furthermore, the mean and variance formulae (Eq. 1) still hold even if $g(\tau)$ is an arbitrary probability density function, for instance, having complex shapes such as multimodality (see Supplementary Texts B and C). The theoretically derived mean time trace (Eq. 1) is consistent with the one obtained numerically (Fig. 2E) (*23*).

Estimation of reaction rates and delay distribution parameters of a single cell

Based on the formulae (Eq. 1), we developed an efficient and scalable Bayesian Markov chain Monte Carlo (MCMC) method, namely, MBI, which estimates probability distributions of the parameters (i.e., posterior distributions) (Fig. 3A) (see Materials and Methods and Supplementary Text D). Specifically, we constructed the Gaussian likelihood function using the mean and variance formulae (Eq. 1) (Fig. 3A, middle). Furthermore, we used the sample mean of the time traces instead of their sample variance to estimate the variance of the likelihood function, because the delayed birth-death process is Poissonian (Eq. 1) and the convergence of the sample mean to the true statistics is faster than that of sample variance (*41*). Thus, from just the mean of the given sample time traces, MBI can estimate posterior distributions of the birth rate, λ_b, death rate, λ_d, and the delay distribution parameters, n and t_r (Fig. 3A, right). Indeed, from the mean of 10^2 sample time traces measured every minute, the posterior samples of all the parameters obtained with MBI successfully capture the true values (Fig. 3, B to D).

When the information of sample time traces is reduced, MBI is still accurate and precise. That is, its accuracy and precision do not decrease even when the sample number is less than 40 (Fig. 3E) or the time interval between observations is similar the mean time delay (fig. S1A). Furthermore, MBI can be applied directly to relatively measured data. Only relative measurements (e.g., relative fluorescence signal) rather than actual molecular counts are typically available. Thus, the mean and variance of the time traces are not the same (i.e., non-Poissonian), which is inconsistent with the underlying Poissonian model (Eq. 1). This mismatch led to a considerable bias in the estimation of the previous inference method for the delayed

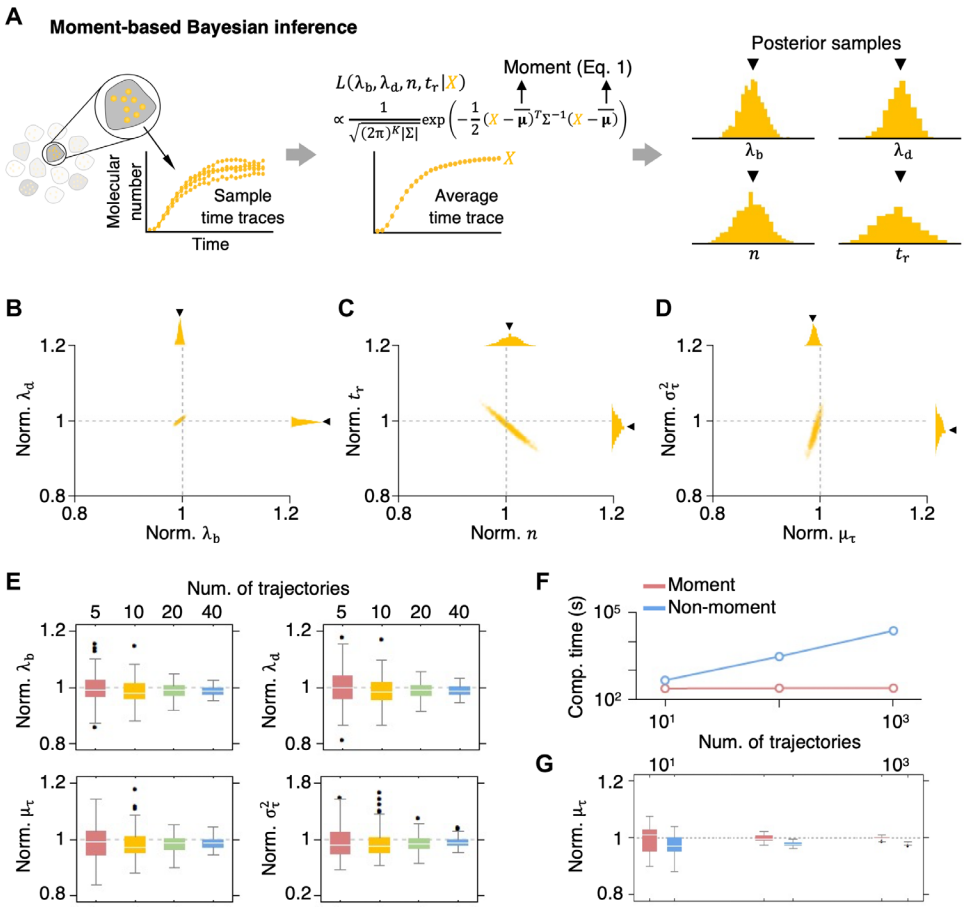

Fig. 3. MBI allows estimation of the reaction rates and time delay parameters of a single cell. (**A**) Schematic diagram of MBI. Multiple sample time traces are measured from a single cell (left). Then, using their average time trace, *X*, we computed the likelihood function, *L*, which was constructed with the mean and variance formulae (Eq. 1) under the Gaussian noise assumption (middle). Σ is a diagonal matrix whose entry is a variance estimate at each time point. Through MCMC sampling with this likelihood function, the posterior samples of parameters are obtained (right). (**B** to **D**) The posterior samples of parameters obtained with MBI using the mean of the sample time traces measured at 1-min intervals in Fig. 2E. The reaction rates (B) and time delay parameters (C and D) were accurately estimated. The sample values were normalized by dividing with the true values of the parameters. (**E**) Box plots of 10^2 posterior means that were obtained using an increasing number of time traces. The estimates were normalized as in (B) to (D). The subsets of between 5 and 40 time traces were randomly and repeatedly selected from the time traces in Fig. 2E. (**F**) This moment-based algorithm is computationally more efficient than the non–moment-based algorithm (*20*) as the number of sample time traces used for the estimation increases. Here, the means of the computation times, which were obtained from 20 individual repetitions of parameter estimation in the setting as in (B) to (D), are shown. (**G**) Box plots of the posterior means obtained from the 20 repetitions. The accuracy and precision are comparable between MBI and the non–moment-based algorithm. Noninformative priors were used throughout these estimations (see Supplementary Text D).

birth-death process (*20*). However, our method can still accurately estimate the parameters (fig. S1, B and C).

Notably, MBI becomes computationally more tractable than the non–moment-based algorithm (*20*) when the number of samples used for the estimation increases (Fig. 3F), while their accuracy and precision are comparable (Fig. 3G). Specifically, even if the number of samples increases, the amount of the information used for the estimation in MBI (i.e., mean) does not increase. Thus, there is no increase in computational cost. In contrast, that of the non–moment-based method increases dramatically when the number of samples increases as it tracks all individual data points.

Estimation of cell-to-cell heterogeneous reaction rates and delay distribution parameters of a cell population

MBI allows one to estimate the reaction rates and the delay distribution parameters of a single cell when a reasonable number of time traces (≥~5) from the single cell is given (Figs. 3 and 4A, i). However, such multiple repetitive measurements in a single cell are challenging with current experimental techniques, because they are time-consuming and potentially alter the properties of the cell and thereby the reaction kinetics (*16*, *17*). Thus, multiple time traces are typically measured with a cell population that is considerably heterogeneous due to large contribution of extrinsic noise (*42*, *43*). In this case, the inference problem is shifted from estimating a parameter set of a single cell to estimating multiple parameter sets of a heterogeneous cell population.

To estimate heterogeneous parameters, we extended MBI with a mixed-effects model, which is a class of statistical models that allows one to analyze the population-level data with extrinsic noise (Fig. 4A, ii; see Supplementary Text E) (*25*). In this extended MBI, all single cells in a heterogeneous population are assumed to share the same model structure (i.e., the delayed birth-death process), and

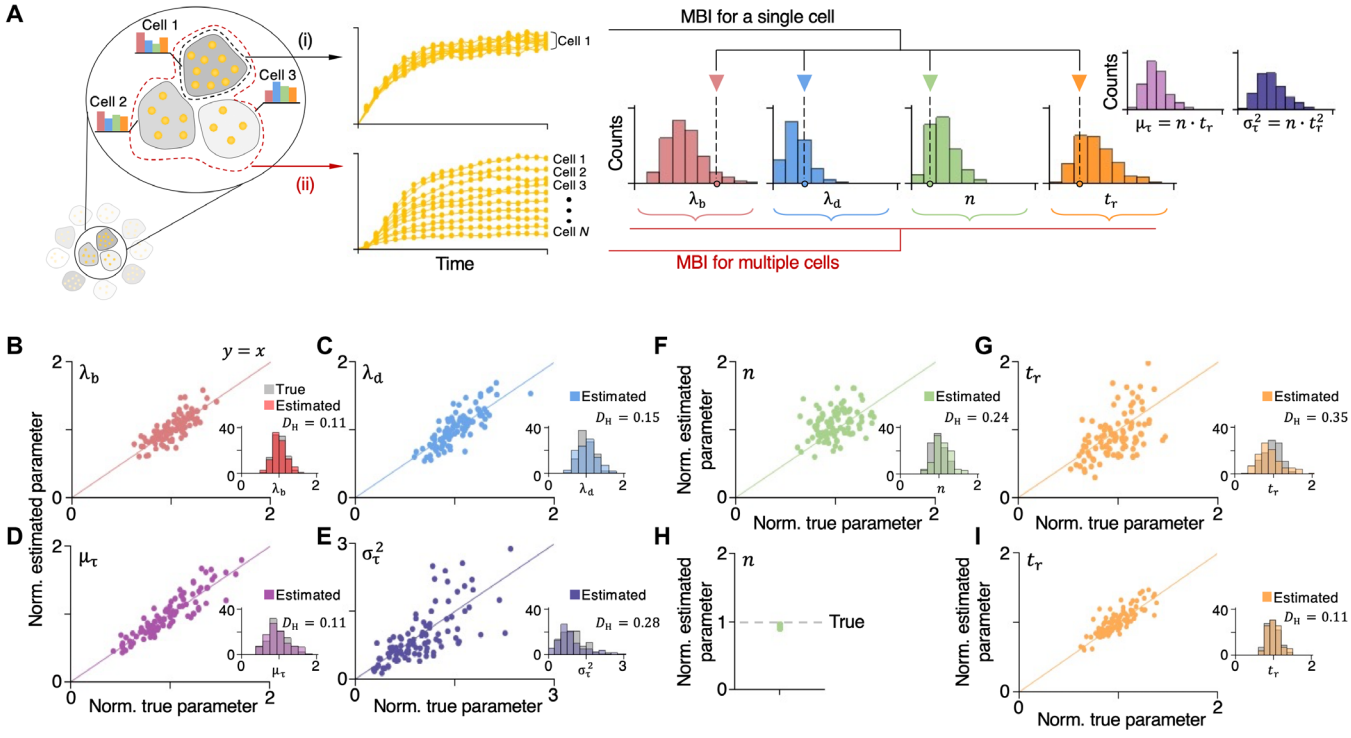

Fig. 4. Bayesian mixed-effects modeling approach allows estimation of cell-to-cell heterogeneous reaction rates and time delay parameters. (**A**) MBI can estimate a single set of parameters from multiple measurements from a single cell (i) or multiple sets of heterogeneous parameters from a single measurement from each single cell in a heterogeneous population (ii). (**B** to **G**) The estimated posterior means of parameters from the 10^2 time traces simulated using 10^2 heterogeneous-delayed birth-death models. The parameter values of the 10^2 models were randomly sampled from gamma distributions whose mean and coefficient of variation are the values in Fig. 2E and 0.2, respectively. The estimates of λ_b (B), λ_d (C), and μ_τ (D) are accurate, and thus their distributions are comparable to those of the true values [inset, (B) to (D)]. However, the estimates of σ_τ^2 (E) are inaccurate due to the inaccurate estimation of n (F) and t_r (G) caused by their strong correlation (fig. S3). The estimated and true parameter values were normalized by dividing by the mean of the true parameters. (**H** and **I**) When 10^2 delayed birth-death models share the same value of n, n (H) and t_r (I) as well as the other parameters (fig. S4) can be accurately and precisely estimated. Here, posterior samples of n (H) and posterior means of t_r (I) are shown. Noninformative priors were used throughout these estimations (see Supplementary Text E).

their difference in responses to an extracellular signal is assumed to originate from different values of the model parameters (i.e., the cell-to-cell heterogeneous birth and death rates and delay distribution parameters), which are distributed following gamma hyper prior distributions (see Supplementary Text E). This allows one to use the information from all single cells in a heterogeneous population together (*25*). Thus, the inference with the mixed-effects model would enable the accurate estimation of parameters even if only one time trace is measured in each single cell in the population.

Indeed, the extended MBI with the mixed-effects model accurately estimated heterogeneous birth rates, λ_b, death rates, λ_d, and mean delays, μ_τ, of the 10^2 delayed birth-death models even when only a single time trace of each model is given (i.e., total of 10^2 time traces) (Fig. 4, B to D). Specifically, the posterior distributions of estimated parameters are similar to those of true parameters [Hellinger distance (D_H) < 0.2] (Fig. 4, B to D, inset). Such accurate estimation is kept when the magnitude of the heterogeneity in the parameters increases, and thus the variation in sample time traces becomes larger (fig. S2).

While an estimated variance of delay, σ_τ^2, of a single cell is accurate when multiple time traces from the single cell are given (Fig. 3D), estimated σ_τ^2 of heterogeneous single cells are inaccurate (Fig. 4E). This is due to the inaccurate estimation of the number of rate-limiting steps, n (Fig. 4F), and the time for each step, t_r (Fig. 4G), caused by their strong correlation leading to their unidentifiability (fig. S3). This identifiability issue might be circumvented by assuming that the number of intermediate rate-limiting steps is the same among single cells, which is reasonable, because the number of intermediate rate-limiting steps in signaling cascades is more likely to be similar among isogenic cells under the same environment compared to the reaction rates. This assumption can be easily incorporated into our method, because it is based on the mixed-effects modeling instead of the traditional naïve two-stage approach that individually estimates parameters (e.g., the rate-limiting step number) of each single cell (*25*), demonstrating an advantage of MBI. Under the assumption, MBI accurately estimated the number of common intermediate rate-limiting steps (Fig. 4H) and the time for each step (Fig. 4I) as well as the other parameters (fig. S4). Furthermore, even when only the relative measurements are available, MBI provides considerably accurate estimation for the magnitude of cell-to-cell heterogeneity (fig. S5).

The magnitude of cell-to-cell heterogeneity in the amplified signal activation rate is positively correlated with the number of intermediate rate-limiting steps

To facilitate the use of MBI, we developed a publicly available computational package of MBI (see Supplementary Text G). Using this computational package, we analyzed the previously measured

single-cell time-lapse yellow fluorescent protein (YFP) expression from the *dnaK* promoter in response to an antibiotic stress, TET, in two *E. coli* colonies (Fig. 5A) (*3*). Because the dilution rate of YFP (λ_d) can be estimated directly from the experimentally measured cell growth rate after antibiotic addition (*3*), we assigned a strongly informative gamma prior for λ_d (see Supplementary Text H). Then, under the assumption that the number of intermediate rate-limiting steps is the same among cells, we estimated the amplified stress signal activation rate (λ_b), the number of rate-limiting steps (n), the time for each step (t_r), and thus the mean signal transduction delay ($\mu_\tau = n \cdot t_r$) (Fig. 5, B to E). The inferred values of parameters showed a considerable magnitude of cell-to-cell heterogeneity (Fig. 5, B to D). The population estimates were similar between the two colonies (Fig. 5, C to E), although the time traces of colony 1 appeared to be

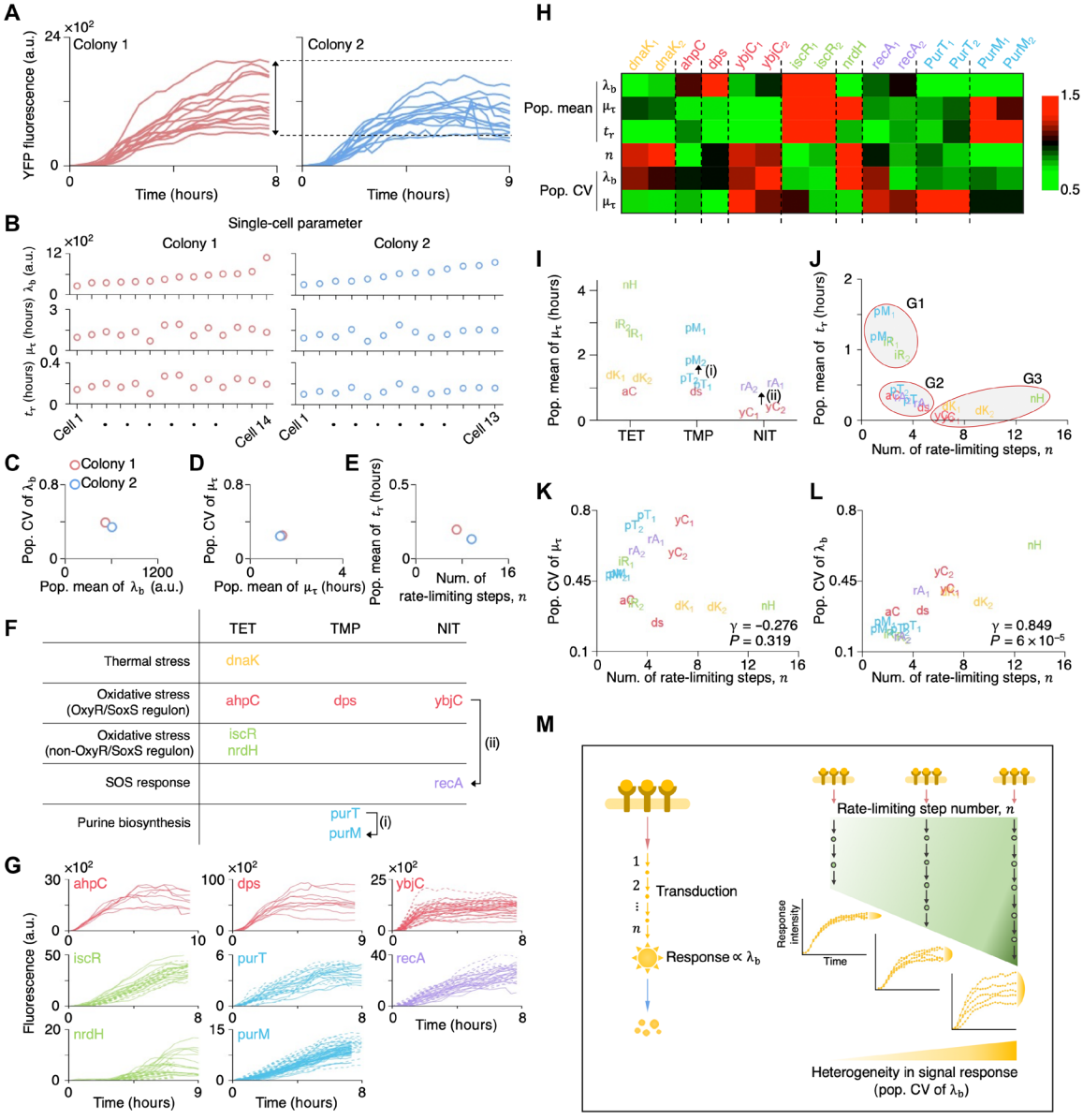

Fig. 5. Rate-limiting step number is positively correlated with the magnitude of heterogeneity in signal response. (**A** and **B**) From single-cell YFP expression from the *dnaK* promoter stimulated by TET (A), the posterior means of single-cell parameters were estimated with MBI (B). a.u., arbitrary units. (**C** and **D**) The mean and coefficient of variation (CV) of the posterior means of λ_b (C) and μ_τ (D). (**E**) The posterior mean of n and the mean of the posterior means of t_r. (**F**) Table describing the antibiotic stresses and their response promoters. The arrows denote the previously reported reaction pathways. (**G**) Single-cell protein expression from the promoters stimulated by the stresses in (F). The solid and dashed lines represent data from two colonies. (**H**) The estimates inferred as in (C) to (E). Here, each estimate normalized by the mean of the estimates is represented by a color ranging from 0.5 (green) to 1.5 (red). If the normalized value is lower than 0.5 or higher than 1.5, then its color is represented by the color for 0.5 or 1.5, respectively. (**I**) The population mean of μ_τ. Abbreviations for the promoter name are as follows: dK, *dnaK*; aC, *ahpC*; iR, *iscR*; nH, *nrdH*; ds, *dps*; pT, *purT*; pM, *purM*; yC, *ybjC*; rA, *recA*. Subscripts denote the index of microcolony. (**J**) The promoters can be classified into three groups, G1, G2, and G3, according to n and mean of t_r. (**K** and **L**) n is not correlated with CV of μ_τ (K) but positively correlated with CV of λ_b (L). γ and P denote the coefficient and P value of Pearson's correlation test, respectively. (**M**) When signal passes through more rate-limiting steps, the cell-to-cell variability in signal response increases.

more heterogeneous than those of colony 2 (Fig. 5A, arrows and dashed lines), supporting the accuracy of MBI even for noisy experimental data.

To investigate how signaling dynamics changes across different antibiotic stresses and response promoters, we applied MBI to the previously measured single-cell time-lapse fluorescent protein expression from other promoters in response to three antibiotic stresses, TET, TMP, and NIT (Fig. 5, F and G; see Supplementary Text H) (*3*). The resulting population estimates were again similar overall between the two colonies (Fig. 5H), demonstrating the accuracy of MBI. The population estimates are considerably heterogeneous, depending on the type of the promoter driving the gene expression and the type of antibiotic (Fig. 5H). Specifically, the population mean of the mean transduction delay varied widely from ~0.3 to ~4.2 hours (Fig. 5I). Notably, the OxyR/SoxS-regulated oxidative stress response (i.e., *ahpC*, *dps*, and *ybjC*) was faster than the other stress responses regardless of which antibiotic stress was given (Fig. 5I). Furthermore, the order of response predicted based on the estimated time delay (*purT* ➔ *purM* and *ybjC* ➔ *recA*; Fig. 5I, i and ii, respectively) matched with previously known reaction orders of purine biosynthesis (Fig. 5F, i) (*44*) and cellular responses to NIT (i.e., oxidative stress response followed by SOS response) (Fig. 5F, ii) (*3*, *45*), respectively. This illustrates that MBI can be used to explore the temporal order of biochemical reactions and cellular responses.

We next compared the number of intermediate rate-limiting steps and the time for each step between the promoters (Fig. 5J). We found that the promoters can be categorized into three groups, G1, G2, and G3, according to the number of intermediate rate-limiting steps and the time for each step (Fig. 5J). Long delays in signal transduction stemmed from either the long-time of each intermediate step (G1) or a large number of short intermediate rate-limiting steps (G3) but not both. We considered whether there might be a difference in the heterogeneity of the time delay depending on whether the delay is generated by a greater number of rate-limiting steps or a longer time of each step. In particular, we hypothesized that a large number of intermediate rate-limiting steps reduces the cell-to-cell variability in delay because the intracellular variability in the transduction delay decreases as the step number increases (*3*, *31*). However, we did not find any significant correlation between them (Fig. 5K), indicating the difference in intracellular and cell-to-cell variability. In contrast, unexpectedly, we found that the magnitude of the cell-to-cell heterogeneity in the amplified signal activation rate is positively correlated with the number of rate-limiting steps (Fig. 5L). This indicates that, as the number of intermediate rate-limiting steps increases, the cell-to-cell variability in signal amplification induced by each intermediate rate-limiting step (*46*) accumulates, leading to the large cell-to-cell variability in the amplified final activation rate ($\lambda_b = \lambda_a \prod_{i=1}^{n} \left(\frac{a_i}{r}\right)$). In this case, cell-to-cell variability in the signal response intensity, mainly determined by λ_b, also increases according to our theoretical calculations (see Supplementary Text I) and exact stochastic simulation (fig. S6). This indicates that the number of rate-limiting steps is a major source of cell-to-cell variability in signal response intensity (Fig. 5M).

Estimation of cell-to-cell heterogeneity for cell signaling processes with feedback regulation

In cell signaling processes, a set of regulatory steps that feeds the output signal back to the input (i.e., a feedback loop) exists ubiquitously (*47*, *48*). For instance, feedback inhibition (Fig. 6A, i) can lead to complex dynamics such as oscillatory signal response that cannot be analyzed using MBI with the delayed birth-death process. To analyze such complex dynamics with MBI, we extended the delayed birth-death process by incorporating feedback inhibition with a fixed delay (τ_2) using the sequestration-based repression function (Fig. 6A, ii) (*49*–*52*). Then, we derived its time-varying exact low-order moments by using a transient Little's law (*39*) and the Chemical Fluctuation Theorem (see Supplementary Text F) (*21*). The theoretically derived mean time trace is consistent with the simulated one (Fig. 6B). Furthermore, MBI based on the formulae allows the accurate estimation of the parameters of a single cell, including ones describing feedback inhibition (fig. S7, A and B). The estimates are still accurate even if sample time traces generated with a random feedback delay were used for estimation, which causes a model misspecification (fig. S7C). Furthermore, MBI with the mixed-effects model, which can be easily used with the computational package (see Supplementary Text G), successfully estimated heterogeneous model parameters (Fig. 6C). Note that, because the derived formulae (Supplementary Text F) are not restricted to the sequestration-based feedback inhibition, MBI can be also used to analyze systems with different types of feedback regulations, including feedback activation.

We next analyzed the previously measured single-cell time-lapse YFP expressions from the *fpr* promoter in response to NIT in two *E. coli* colonies that show adaptation behaviors, indicating the presence of the feedback inhibition (Fig. 6D) (*3*). The inferred population estimates were similar overall between the colonies (Fig. 6E), indicating the accuracy of MBI even for the system with the feedback. We next applied our method to the previously measured single-cell time-lapse fluorescent protein expression from various promoters in response to four antibiotic stresses, TET, TMP, NIT, and CHL (Fig. 6F and fig. S8) (see Supplementary Text H) (*2*). Our inference results identified that the dynamics of output response depend on the mean of total time delay of signal transduction and feedback ($\mu_{\tau_1+\tau_2}$) and the ratio between birth rate and the abundance of output molecules to achieve maximum repression (λ_b/R), representing the repression intensity (Fig. 6F and fig. S8B). Specifically, when both $\mu_{\tau_1+\tau_2}$ and λ_b/R are small, stress responses would monotonically increase and then be saturated with small fluctuation (*rmuC*; Fig. 6F, i). As $\mu_{\tau_1+\tau_2}$ becomes large, adaptation with a long duration occurs (*ychF*; Fig. 6F, ii). When λ_b/R becomes large, signal response intensity shows oscillations (*ycfR*; Fig. 6F, iii), and the period becomes longer with larger $\mu_{\tau_1+\tau_2}$ (*hemB*; Fig. 6F, iv). These results illustrate the usefulness of MBI to understand the dynamics underlying output measurements. In this analysis (Fig. 6F), we were not able to infer cell-to-cell variability, because a single time trace was given for each promoter. Thus, we performed an in silico experiment, indicating that the rate-limiting step number is again the source of cell-to-cell variability even for the non-Poissonian process with the feedback inhibition (fig. S9).

DISCUSSION

In this work, we developed MBI that can infer cell-to-cell heterogeneity in amplified activation rate, signal transduction time, feedback inhibition time, and signal decay rate from only the time traces of the final signal response (Figs. 3 to 6 and figs. S1 to S5, S7, and S8). In particular, without tracking intermediate steps experimentally, our method can infer the number of intermediate rate-limiting steps and the time of each step. This allowed us to classify the stress response promoters to three antibiotic stresses (i.e., TET,

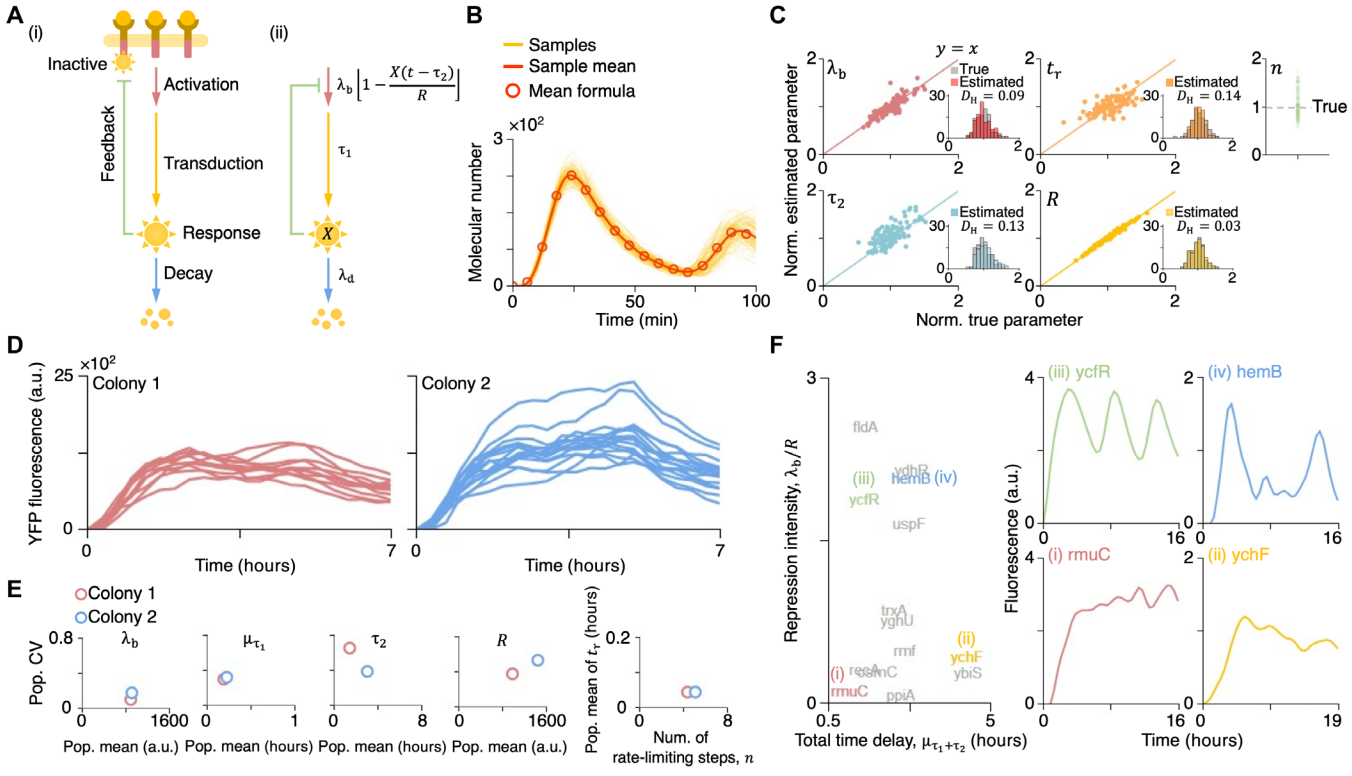

Fig. 6. MBI can be used to analyze cell signaling processes with feedback inhibition. (**A**) Signaling process with feedback inhibition. The feedback inhibition is incorporated into the delayed birth-death process (Fig. 2D). The output response molecules (*X*) self-inhibit their expression via interaction with input molecules, which is modeled as a delayed sequestration-based repression function $\left|1-\frac{X(t-\tau_2)}{R}\right|$, where *R* is the abundance of output molecules to achieve maximum repression, τ_2 is a fixed time delay for the feedback inhibition, and $\lfloor f \rfloor$ is maximum of *f* and 0. (**B**) The mean of the molecular number of the model calculated by the formula (red circle) is the same as that of simulated 10^2 sample time traces (red line). Here, $\lambda_b = 30\ \text{min}^{-1}$, $\lambda_d = 0.05\ \text{min}^{-1}$, $\tau_1 \sim \Gamma(n=5,\ t_r = 2\ \text{min}^{-1})$, $R = 50$, and $\tau_2 = 5$ min. (**C**) The estimated posterior means of parameters of 10^2 heterogeneous models with feedback inhibition. The parameters were estimated as in Fig. 4 (B to I). The dilution rate (λ_d) was given, as it can be directly estimated from the experimentally measured cell growth rate. (**D**) Single-cell YFP expression time traces from the *fpr* promoter in two colonies stimulated by NIT. (**E**) The population estimates of the parameters are similar between the two colonies. (**F**) The posterior means of the total delay, $\mu_{\tau_1+\tau_2}$, and the repression intensity, λ_b/R. See fig. S8 for details.

TMP, and NIT) based on the number of rate-limiting steps and the time of each step. Throughout the classification, we found that the long time delay stems from either a large number of steps or a long time of each step but not both (Fig. 5J). We also found the counter-intuitive discrepancy between intracellular and cell-to-cell variability in signaling dynamics: While the intracellular variability in the transduction delay decreases as the rate-limiting step number increases (*3*, *31*), the cell-to-cell variability does not change (Fig. 5K). Furthermore, we found that as the number of rate-limiting steps increases, the magnitude of the cell-to-cell heterogeneity in signal activation rate, determining the strength of signal response, increases (Fig. 5, L and M). This relationship is preserved for Poissonian-delayed birth-death processes having any heterogeneous cell-to-cell parameter distribution (see Supplementary Text I), which is expandable to the non-Poissonian process with feedback regulation according to an in silico experiment (fig. S9). It would be interesting in future work to investigate whether the property can be extended to diverse systems, for instance, having multimodal dynamics such as a toggle switch network with arbitrary waiting time distributions (*22*, *53*, *54*).

The delayed birth-death process used in this study can describe fundamental reaction networks, such as signaling cascades (Figs. 2A and 6A) and mature protein synthesis (Fig. 2B) (*18*–*20*, *35*, *37*). However, this model has a limitation. For instance, protein dilution is modeled as a first-order reaction, and the consecutive signal activation is used. This might not accurately describe their contribution to extrinsic cell-to-cell variability (*55*, *56*). To tackle this, more realistic dilution reflecting cell division and signal activation via a bursty reaction are needed to be incorporated into the delayed model as in previous work (fig. S10) (*55*–*57*). Even when these mechanisms are incorporated into the model, we can derive the formulae describing the model dynamics (see Supplementary Text J). It would be interesting to use our framework with the formulae to systematically analyze the contribution of cell division or bursty expression to extrinsic cell-to-cell variability. For more complex reaction networks, moments could be derived with the Little's Law (*39*), the Chemical Fluctuation Theorem (*21*), Wiener-Khinchin Theorem (*56*), or Lindley's integral equation (*40*). Moreover, a theory, which converts a non-Markovian system with time delay into a topology-equivalent Markovian system by introducing effective transition rate decoding the effect of non-Markovian processes, could also be used (*22*, *58*).

Since our method is only based on the low-order moments, it is computationally more efficient than methods tracking all individual data points (Fig. 3F). However, for complex systems, estimation using low-order moments can be biased as it exploits only partial information of the system. This issue could be resolved by tracking all individual data points in the inference (*59*), which would be interesting in future work. Another important piece of follow-up research is to

generalize the gamma hyper prior assumption of the mixed-effects model used in our and previous studies (*25*, *60*), because this makes it challenging to capture the multimodality of population distributions (*61*). In this case, one can use a maximum entropy-based framework that exploits data-derived constraints to derive the parameter distribution rather than enforcing a specific one (*62*). An interesting avenue for further work is to combine the maximum entropy-based framework with our moment-based method. To use MBI more accurately, identifying a specific model that successfully captures a system structure (e.g., delayed birth-death process) is a prerequisite. For this, various network inference methods (*63*–*65*) can be used.

The heterogeneous mean signal transduction delays can be accurately inferred by using our user-friendly computational package even from noisy experimental time series data (Fig. 5, B, D, H, and I). The inferred delays can provide valuable information to identify the temporal order of biochemical reactions and single-cell responses to an extracellular stimulus (Fig. 5, F and I). Furthermore, this can assist identification of whether adaptation to a stressful environment (e.g., oxidative stress) offers a tolerance or resistance to other stresses (e.g., DNA damage stress), i.e., cross-protection (Fig. 5, H and I) (*3*, *45*). In particular, our method can be used to find hidden cross-protection relationships between cellular stresses (e.g., acid stress and thermal stress) (*66*) or between virus infections (e.g., Dengue and Zika) (*67*). We also identified that the cell-to-cell variability in the strength of response to antibiotic drugs accumulates as the signal passes through more rate-limiting steps (Fig. 5, L and M). This indicates that an increase in the number of rate-limiting steps that lie between the application of the drugs and the therapeutic response increases the variability of the efficacy. Given this, the rate-limiting step number, which can be estimated by our method, appears to be critical information for selecting target molecules for drug development. Our result can also facilitate the precision medicine as it allows for the systematic understanding of the heterogeneity of treatment effects, which is a big challenge in precision medicine (*68*).

MATERIALS AND METHODS

Derivation of low-order moments for signaling processes and MBI with the derived moments

We derived the mean, $\mu(t;\Theta)$, and variance, $\sigma^2(t;\Theta)$, for the delayed birth-death process (Fig. 2D; see Supplementary Texts B and C) and the one with feedback regulation (Fig. 6A; see Supplementary Text F) where Θ is the set of parameters. Then, as done in previous work (*69*), the likelihood function of Θ for given data $\mathbf{x} = (x_{t1}, \ldots, x_{tK})$ is constructed as

$$L(\Theta \mid \mathbf{x}) = \prod_{i=1}^{K} p\left(x_{t_i} \mid \tilde{\mu}(t_i), \tilde{\sigma}^2(t_i)\right)$$

where $p(x \mid \mu, \sigma^2)$ is the probability density function of the normal distribution with mean μ and variance σ^2, and the $\tilde{\mu}$ and $\tilde{\sigma}^2$ were calculated using the derived moments (see Supplementary Texts D to F for details). This likelihood function was used to estimate parameters for a single cell (Fig. 3, A to E, and fig. S7; see Supplementary Texts D and F). Then, it was exploited with a mixed-effects modeling approach to estimate parameters for a heterogeneous cell population (Figs. 4 and 6C; see Supplementary Texts E and F). This developed inference framework can be easily implemented via our publicly available and user-friendly computational package (see Supplementary Text G for the step-by-step protocol; https://doi.org/10.5281/zenodo.5904961).

Simulation

All the simulations were performed using R version 4.0.5 with a computer cluster composed of seven machines where each machine is equipped with two Intel Xeon SP-6148 CPUs (2.4 GHz, 20C), 192-GB RAM, and the operating system CentOS 7.4, 64 bit.

Statistical analysis

Pearson correlation coefficients and the corresponding *P* values in Fig. 5 (K and L) were calculated using Mathematica.

Box 1. Glossary.

Bayesian inference: Statistical inference method to update our prior beliefs about events when new information becomes available (*41*). In this study, an event represents that cell signaling parameters [$\theta = (\lambda_b, \lambda_d, n, t_r, R, \tau_2)$] have certain values, and prior beliefs are our initial beliefs about the parameter values (i.e., prior distributions) when any information is unavailable. The new information is sample time traces measured from single cells ($\mathbf{x}$). See Supplementary Texts D and E for details.

Chemical Fluctuation Theorem: Mathematical theorem that provides the exact time-varying relationship between the fluctuation in the molecular number (i.e., the variance of molecular number) and the dynamics of creation and degradation processes of molecules. See (*21*) and Supplementary Text C for details.

Chemical master equation: Equation providing the probabilistic description of chemical reaction systems (e.g., the delayed birth-death process in Fig.2D) (*27*). In the equation, the system state is given by the molecular numbers. The probability of being in a certain state at a given time is governed by the equation.

Hellinger distance: A metric to measure the difference between two probability distributions. If the two distributions are identical, then the Hellinger distance is zero. If they are completely different, then the distance is one.

Likelihood function: Function to measure how well given beliefs explains given information (*41*). See Supplementary Texts D and E for details.

Markovian and non-Markovian systems: A Markovian system is a random process in which the future state is only dependent on the present. A non-Markovian system is a random process in which the future state is dependent on the past as well as the present.

MCMC methods: Methods to sample from a probability distribution, which is typically high dimensional. Samples from the desired distribution are obtained by recording the states of a Markovian system whose stationary distribution is the desired distribution. See Supplementary Texts D and E for details.

Mixed-effects model: A statistical framework for exploring variability between individuals in a population. It allows making use of population-level data together, when inferring an individual parameter. Thus, it helps to circumvent the uncertainty problem in parameter estimation, which is caused by the lack of information. See (*25*) and Supplementary Text E for details.

Moments: A set of statistical parameters determining the shape of the probability distribution. The *k*th moment of a random variable is the expected value of its *k*th power. Thus, the first moment is the mean, and the second moment subtracted by the first moment squared is the variance.

Transient Little's law: Mathematical theorem that provides the exact time-varying relationship between the mean number of molecules and the dynamics of creation and degradation processes of molecules. See (*39*) and Supplementary Text B for details.

SUPPLEMENTARY MATERIALS

Supplementary material for this article is available at https://science.org/doi/10.1126/sciadv.abl4598

View/request a protocol for this paper from *Bio-protocol*.

REFERENCES AND NOTES

1. A. Raj, A. Van Oudenaarden, Nature, nurture, or chance: Stochastic gene expression and its consequences. *Cell* **135**, 216–226 (2008).
2. K. Mitosch, G. Rieckh, T. Bollenbach, Noisy response to antibiotic stress predicts subsequent single-cell survival in an acidic environment. *Cell Syst.* **4**, 393–403.e5 (2017).
3. K. Mitosch, G. Rieckh, T. Bollenbach, Temporal order and precision of complex stress responses in individual bacteria. *Mol. Syst. Biol.* **15**, e8470 (2019).
4. M. Niepel, S. L. Spencer, P. K. Sorger, Non-genetic cell-to-cell variability and the consequences for pharmacology. *Curr. Opin. Chem. Biol.* **13**, 556–561 (2009).
5. B. R. Levin, D. E. Rozen, Non-inherited antibiotic resistance. *Nat. Rev. Microbiol.* **4**, 556–562 (2006).
6. Y. Wakamoto, N. Dhar, R. Chait, K. Schneider, F. Signorino-Gelo, S. Leibler, J. D. McKinney, Dynamic persistence of antibiotic-stressed mycobacteria. *Science* **339**, 91–95 (2013).
7. A. Raj, S. A. Rifkin, E. Andersen, A. Van Oudenaarden, Variability in gene expression underlies incomplete penetrance. *Nature* **463**, 913–918 (2010).
8. P. B. Gupta, I. Pastushenko, A. Skibinski, C. Blanpain, C. Kuperwasser, Phenotypic plasticity: Driver of cancer initiation, progression, and therapy resistance. *Cell Stem Cell* **24**, 65–78 (2019).
9. S. Di Talia, J. M. Skotheim, J. M. Bean, E. D. Siggia, F. R. Cross, The effects of molecular noise and size control on variability in the budding yeast cell cycle. *Nature* **448**, 947–951 (2007).
10. M. Wallden, D. Fange, E. G. Lundius, O. Baltekin, J. Elf, The synchronization of replication and division cycles in individual *E. coli* cells. *Cell* **166**, 729–739 (2016).
11. B. B. Aldridge, M. Fernandez-Suarez, D. Heller, V. Ambravaneswaran, D. Irimia, M. Toner, S. M. Fortune, Asymmetry and aging of mycobacterial cells lead to variable growth and antibiotic susceptibility. *Science* **335**, 100–104 (2012).
12. J. Yang, M. Reth, Oligomeric organization of the B-cell antigen receptor on resting cells. *Nature* **467**, 465–469 (2010).
13. S. Yang, S. Kim, Y. R. Lim, C. Kim, H. J. An, H.-H. Kim, J. Sung, N. K. Lee, Contribution of RNA polymerase concentration variation to protein expression noise. *Nat. Commun.* **5**, 4761 (2014).
14. P. Pozarowski, Z. Darzynkiewicz, Analysis of Cell Cycle by Flow Cytometry, in *Checkpoint controls and cancer*, A. H. Schönthal, Ed. (Springer, 2004), vol. 281, chap. 22. pp. 301–311.
15. A. Sarrion-Perdigones, L. Chang, Y. Gonzalez, T. Gallego-Flores, D. W. Young, K. J. T. Venken, Examining multiple cellular pathways at once using multiplex hextuple luciferase assaying. *Nat. Commun.* **10**, 1710 (2019).
16. I. C. Macaulay, C. P. Ponting, T. Voet, Single-cell multiomics: Multiple measurements from single cells. *Trends Genet.* **33**, 155–168 (2017).
17. J. Yu, J. Zhou, A. Sutherland, W. Wei, Y. S. Shin, M. Xue, J. R. Heath, Microfluidics-based single-cell functional proteomics for fundamental and applied biomedical applications. *Ann. Rev. Anal. Chem.* **7**, 275–295 (2014).
18. M. Barrio, A. Leier, T. T. Marquez-Lago, Reduction of chemical reaction networks through delay distributions. *J. Chem. Phys.* **138**, 104114 (2013).
19. M. Beguerisse-Díaz, R. Desikan, M. Barahona, Linear models of activation cascades: Analytical solutions and coarse-graining of delayed signal transduction. *J. R. Soc. Interface* **13**, 20160409 (2016).
20. B. Choi, Y. Y. Cheng, S. Cinar, W. Ott, M. R. Bennett, K. Josić, J. K. Kim, Bayesian inference of distributed time delay in transcriptional and translational regulation. *Bioinformatics* **36**, 586–593 (2020).
21. S. J. Park, S. Song, G. S. Yang, P. M. Kim, S. Yoon, J. H. Kim, J. Sung, The chemical fluctuation theorem governing gene expression. *Nat. Commun.* **9**, 297 (2018).
22. J. Zhang, T. Zhou, Markovian approaches to modeling intracellular reaction processes with molecular memory. *Proc. Natl. Acad. Sci. U.S.A.* **116**, 23542–23550 (2019).
23. C. Gupta, J. M. López, R. Azencott, M. R. Bennett, K. Josić, W. Ott, Modeling delay in genetic networks: From delay birth-death processes to delay stochastic differential equations. *J. Chem. Phys.* **140**, 204108 (2014).
24. C. Gardiner, *Stochastic Methods* (Springer, 2009), vol. 4.
25. M. Karlsson, D. L. I. Janzén, L. Durrieu, A. Colman-Lerner, M. C. Kjellsson, G. Cedersund, Nonlinear mixed-effects modelling for single cell estimation: When, why, and how to use it. *BMC Syst. Biol.* **9**, 52 (2015).
26. J. Almquist, L. Bendrioua, C. B. Adiels, M. Goksör, S. Hohmann, M. Jirstrand, A nonlinear mixed effects approach for modeling the cell-to-cell variability of Mig1 dynamics in yeast. *PLOS ONE* **10**, e0124050 (2015).
27. D. Schnoerr, G. Sanguinetti, R. Grima, Approximation and inference methods for stochastic biochemical kinetics—A tutorial review. *J. Phys. A: Math. Theor.* **50**, 093001 (2017).
28. C. Zechner, J. Ruess, P. Krenn, S. Pelet, M. Peter, J. Lygeros, H. Koeppl, Moment-based inference predicts bimodality in transient gene expression. *Proc. Natl. Acad. Sci. U.S.A.* **109**, 8340–8345 (2012).
29. A. Leier, T. T. Marquez-Lago, Delay chemical master equation: Direct and closed-form solutions. *Proc. R. Soc. A: Math. Phys. Eng. Sci.* **471**, 20150049 (2015).
30. S. Calderazzo, M. Brancaccio, B. Finkenstadt, Filtering and inference for stochastic oscillators with distributed delays. *Bioinformatics* **35**, 1380–1387 (2019).
31. J. R. Moffitt, C. Bustamante, Extracting signal from noise: Kinetic mechanisms from a Michaelis–Menten-like expression for enzymatic fluctuations. *FEBS J.* **281**, 498–517 (2014).
32. J. Roux, M. Hafner, S. Bandara, J. J. Sims, H. Hudson, D. Chai, P. K. Sorger, Fractional killing arises from cell-to-cell variability in overcoming a caspase activity threshold. *Mol. Syst. Biol.* **11**, 803 (2015).
33. B. N. Kholodenko, Cell-signalling dynamics in time and space. *Nat. Rev. Mol. Cell Biol.* **7**, 165–176 (2006).
34. R. A. Bradshaw, E. A. Dennis, *Handbook of Cell Signaling* (Academic press, 2009).
35. N. Korsbo, H. Jönsson, It's about time: Analysing simplifying assumptions for modelling multi-step pathways in systems biology. *PLoS Comput. Biol.* **16**, e1007982 (2020).
36. E. Balleza, J. M. Kim, P. Cluzel, Systematic characterization of maturation time of fluorescent proteins in living cells. *Nat. Methods* **15**, 47–51 (2018).
37. A. Leier, M. Barrio, T. T. Marquez-Lago, Exact model reduction with delays: Closed-form distributions and extensions to fully bi-directional monomolecular reactions. *J. R. Soc. Interface* **11**, 20140108 (2014).
38. Y. Y. Cheng, A. J. Hirning, K. Josic, M. R. Bennett, The timing of transcriptional regulation in synthetic gene circuits. *ACS Synth. Biol.* **6**, 1996–2002 (2017).
39. D. Bertsimas, G. Mourtzinou, Transient laws of non-stationary queueing systems and their applications. *Queueing Syst.* **25**, 115–155 (1997).
40. L. Kleinrock, *Queueing Systems* (Wiley, 1975).
41. W. J. Dixon, F. J. Massey Jr., *Introduction to Statistical Analysis* (1951).
42. S. Tanase-Nicola, P. B. Warren, P. R. ten Wolde, Signal detection, modularity, and the correlation between extrinsic and intrinsic noise in biochemical networks. *Phys. Rev. Lett.* **97**, 068102 (2006).
43. J. Selimkhanov, B. Taylor, J. Yao, A. Pilko, J. Albeck, A. Hoffmann, L. Tsimring, R. Wollman, Systems biology. Accurate information transmission through dynamic biochemical signaling networks. *Science* **346**, 1370–1373 (2014).
44. A. Cersini, M. C. Martino, I. Martini, G. Rossi, M. L. Bernardini, Analysis of virulence and inflammatory potential of Shigella flexneri purine biosynthesis mutants. *Infect. Immun.* **71**, 7002–7013 (2003).
45. D. W. Bryant, D. R. McCalla, Nitrofuran induced mutagenesis and error prone repair in Escherichia coli. *Chem. Biol. Interact.* **31**, 151–166 (1980).
46. S. Sonneveld, B. M. Verhagen, M. E. Tanenbaum, Heterogeneity in mRNA translation. *Trends Cell Biol.* **30**, 606–618 (2020).
47. O. Brandman, T. Meyer, Feedback loops shape cellular signals in space and time. *Science* **322**, 390–395 (2008).
48. V. Shimoga, J. T. White, Y. Li, E. Sontag, L. Bleris, Synthetic mammalian transgene negative autoregulation. *Mol. Syst. Biol.* **9**, 670 (2013).
49. J. K. Kim, J. J. Tyson, Misuse of the Michaelis–Menten rate law for protein interaction networks and its remedy. *PLoS Comput. Biol.* **16**, e1008258 (2020).
50. J. K. Kim, Protein sequestration versus Hill-type repression in circadian clock models. *IET Syst. Biol.* **10**, 125–135 (2016).
51. Y. M. Song, H. Hong, J. K. Kim, Universally valid reduction of multiscale stochastic biochemical systems using simple non-elementary propensities. *PLoS Comput. Biol.* **17**, e1008952 (2021).
52. S. Beesley, D. W. Kim, M. D'Alessandro, Y. Jin, K. Lee, H. Joo, Y. Young, R. J. Tomko Jr., J. Faulkner, J. Gamsby, J. K. Kim, C. Lee, Wake-sleep cycles are severely disrupted by diseases affecting cytoplasmic homeostasis. *Proc. Natl. Acad. Sci. U.S.A.* **117**, 28402–28411 (2020).
53. T. Zhou, T. Liu, Quantitative analysis of gene expression systems. *Quant. Biol.* **3**, 168–181 (2015).
54. H. Hong, J. Kim, M. A. Al-Radhawi, E. D. Sontag, J. K. Kim, Derivation of stationary distributions of biochemical reaction networks via structure transformation. *Commun. Biol.* **4**, 1–10 (2021).
55. C. H. Beentjes, R. Perez-Carrasco, R. Grima, Exact solution of stochastic gene expression models with bursting, cell cycle and replication dynamics. *Phys. Rev. E* **101**, 032403 (2020).
56. C. Jia, R. Grima, Frequency domain analysis of fluctuations of mRNA and protein copy numbers within a cell lineage: Theory and experimental validation. *Phys. Rev. X* **11**, 021032 (2021).
57. Z. Cao, R. Grima, Analytical distributions for detailed models of stochastic gene expression in eukaryotic cells. *Proc. Natl. Acad. Sci. U.S.A.* **117**, 4682–4692 (2020).

58. Q. Jiang, X. Fu, S. Yan, R. Li, W. Du, Z. Cao, F. Qian, R. Grima, Neural network aided approximation and parameter inference of non-Markovian models of gene expression. *Nat. Commun.* **12**, 2618 (2021).
59. M. J. Cortez, H. Hong, B. Choi, J. K. Kim, K. Josić, Hierarchical Bayesian models of transcriptional and translational regulation processes with delays. *Bioinformatics* **38**, 187–195 (2021).
60. C. Zechner, M. Unger, S. Pelet, M. Peter, H. Koeppl, Scalable inference of heterogeneous reaction kinetics from pooled single-cell recordings. *Nat. Methods* **11**, 197–202 (2014).
61. A. P. Frei, F. A. Bava, E. R. Zunder, E. W. Y. Hsieh, S. Y. Chen, G. P. Nolan, P. F. Gherardini, Highly multiplexed simultaneous detection of RNAs and proteins in single cells. *Nat. Methods* **13**, 269–275 (2016).
62. P. D. Dixit, E. Lyashenko, M. Niepel, D. Vitkup, Maximum entropy framework for predictive inference of cell population heterogeneity and responses in signaling networks. *Cell Syst.* **10**, 204–212.e8 (2020).
63. K. Sachs, O. Perez, D. Pe'er, D. A. Lauffenburger, G. P. Nolan, Causal protein-signaling networks derived from multiparameter single-cell data. *Science* **308**, 523–529 (2005).
64. D. Pe'er, A. Regev, G. Elidan, N. Friedman, Inferring subnetworks from perturbed expression profiles. *Bioinformatics* **17**, S215–S224 (2001).
65. J. Tyler, D. Forger, J. K. Kim, Inferring causality in biological oscillators. *Bioinformatics* **38**, 196–203 (2021).
66. L. U. Haberbeck, X. Wang, C. Michiels, F. Devlieghere, M. Uyttendaele, A. H. Geeraerd, Cross-protection between controlled acid-adaptation and thermal inactivation for 48 *Escherichia coli* strains. *Int. J. Food Microbiol.* **241**, 206–214 (2017).
67. R. Wang, N. Gao, Y. Li, D. Fan, Z. Zhen, K. Feng, H. Chen, J. An, Cross-protection against four serotypes of dengue virus in mice conferred by a Zika DNA vaccine. *Front. Cell. Infect. Microbiol.* **9**, 147 (2019).
68. J. S. Gewandter, M. P. McDermott, H. He, S. Gao, X. Cai, J. T. Farrar, N. P. Katz, J. D. Markman, S. Senn, D. C. Turk, R. H. Dworkin, Demonstrating heterogeneity of treatment effects among patients: An overlooked but important step toward precision medicine. *Clin. Pharmacol. Ther.* **106**, 204–210 (2019).
69. J. Liu, D. Hansen, E. Eck, Y. J. Kim, M. Turner, S. Alamos, H. G. Garcia, Real-time single-cell characterization of the eukaryotic transcription cycle reveals correlations between RNA initiation, elongation, and cleavage. *PLoS Comput. Biol.* **17**, e1008999 (2021).
70. C. J. Geyer, Practical markov chain monte carlo. *Stat. Sci.* **7**, 473–483 (1992).
71. D. Barber, Y. Wang, in *International Conference on Machine Learning* (PMLR, 2014), 1485–1493.
72. A. F. Smith, G. O. Roberts, Bayesian computation via the Gibbs sampler and related Markov chain Monte Carlo methods. *J. R. Stat. Soc. Series. B Stat. Methodol.* **55**, 3–23 (1993).
73. W. K. Hastings, Monte Carlo sampling methods using Markov chains and their applications. *Biometrika* **57**, 97–109 (1970).
74. S. G. Eick, W. A. Massey, W. Whitt, The physics of the $M_t/G/\infty$ queue. *Oper. Res.* **41**, 731–742 (1993).
75. R. Milo, R. Phillips, *Cell Biology by the Numbers* (Garland Science, 2015).
76. R. Perez-Carrasco, C. Beentjes, R. Grima, Effects of cell cycle variability on lineage and population measurements of messenger RNA abundance. *J. R. Soc. Interface* **17**, 20200360 (2020).
77. P. Wang, S. Hayden, Y. Masui, Transition of the blastomere cell cycle from cell size-independent to size-dependent control at the midblastula stage in *Xenopus laevis*. *J. Exp. Zool.* **287**, 128–144 (2000).
78. J. M. Pedraza, J. Paulsson, Effects of molecular memory and bursting on fluctuations in gene expression. *Science* **319**, 339–343 (2008).
79. C. R. Bartman, N. Hamagami, C. A. Keller, B. Giardine, R. C. Hardison, G. A. Blobel, A. Raj, Transcriptional burst initiation and polymerase pause release are key control points of transcriptional regulation. *Mol. Cell* **73**, 519–532..e4 (2019).
80. Y. Taniguchi, P. J. Choi, G.-W. Li, H. Chen, M. Babu, J. Hearn, A. Emili, X. S. Xie, Quantifying *E. coli* proteome and transcriptome with single-molecule sensitivity in single cells. *Science* **329**, 533–538 (2010).
81. V. Shahrezaei, P. S. Swain, Analytical distributions for stochastic gene expression. *Proc. Natl. Acad. Sci. U.S.A.* **105**, 17256–17261 (2008).
82. L. Liu, B. Kashyap, J. Templeton, On the $GI^X/G/\infty$ system. *J. Appl. Prob.* **27**, 671–683 (1990).

Acknowledgments: We thank J. Sung for valuable comments and Life Science Editors for editing support. We thank T. Bollenbach, K. Mitosch, and G. Rieckh for sharing their previously published experimental data and providing detailed information about the data. **Funding:** This work was supported by Samsung Science and Technology Foundation SSTF-BA1902-01 (to J.K.K.), Institute for Basic Science IBS-R029-C3 (to J.K.K.), NRF-2017-Fostering Core Leaders of the Future Basic Science Program/Global Ph.D. Fellowship Program 2017H1A2A1046381 (to D.W.K.), and NRF-2019-Fostering Core Leaders of the Future Basic Science Program/Global Ph.D. Fellowship Program 2019H1A2A1075303 (to H.H.). **Author contributions:** Conceptualization: J.K.K., D.W.K., and H.H. Methodology: J.K.K., D.W.K., and H.H. Investigation: D.W.K. and H.H. Supervision: J.K.K. Writing—original draft: J.K.K. and D.W.K. Writing—review and editing: J.K.K., D.W.K., and H.H. **Competing interests:** The authors declare that they have no competing interests. **Data and materials availability:** All data needed to evaluate the conclusions in the paper are present in the paper and/or the Supplementary Materials. The R codes used for inference are available online (Zenodo: https://doi.org/10.5281/zenodo.5904961; GitHub: https://github.com/Mathbiomed/MBI). The time-lapse microscopy data used in Figs. 5 and 6 (D and E) are publicly available on the website in (*3*), and the data used in Fig. 6F and fig. S8 are publicly available on the website in (*2*).

Submitted 14 July 2021
Accepted 26 January 2022
Published 18 March 2022
10.1126/sciadv.abl4598